This is the accepted version of the paper Rizzotto Francesco, Vasiljevic Zorka Z., Stanojevic Gordana, Dojcinovic Milena P., Jankovic-Castvan Ivona, Vujancevic Jelena D., Tadic Nenad B., Brankovic Goran O., Magniez Aurélie, Vidic Jasmina, Nikolic Maria Vesna "Antioxidant and Cell-friendly Fe_2TiO_5 Nanoparticles for Food Packaging Application" in Food Chemistry 390(2022) 133198 https://doi.org/10.1016/j.foodchem.2022.133198

Antioxidant and Cell-friendly Fe_2TiO_5 Nanoparticles for Food Packaging Application

Francesco Rizzotto[1], Zorka Z. Vasiljevic[2], Gordana Stanojevic[2], Milena P. Dojcinovic[2], Ivona Jankovic-Castvan[3], Jelena D. Vujancevic[4], Nenad B. Tadic[5], Goran O. Brankovic[2], Aurélie Magniez[1], Jasmina Vidic[1,*], Maria Vesna Nikolic[2,*]

[1] Université Paris-Saclay, Micalis Institute, INRAE, AgroParisTech, 78350 Jouy-en-Josas, France

[2] University of Belgrade - Institute for Multidisciplinary Research, 11030 Belgrade, Serbia

[3]University of Belgrade, Faculty of Technology and Metallurgy, 11000 Belgrade, Serbia

[4]Institute of Technical Sciences of SASA, 11000 Belgrade, Serbia

[5]University of Belgrade, Faculty of Physics, 11000 Belgrade, Serbia

Correspondence: J.V. jasmina.vidic@inrae.fr and M.V.N. mariavesna@imsi.rs

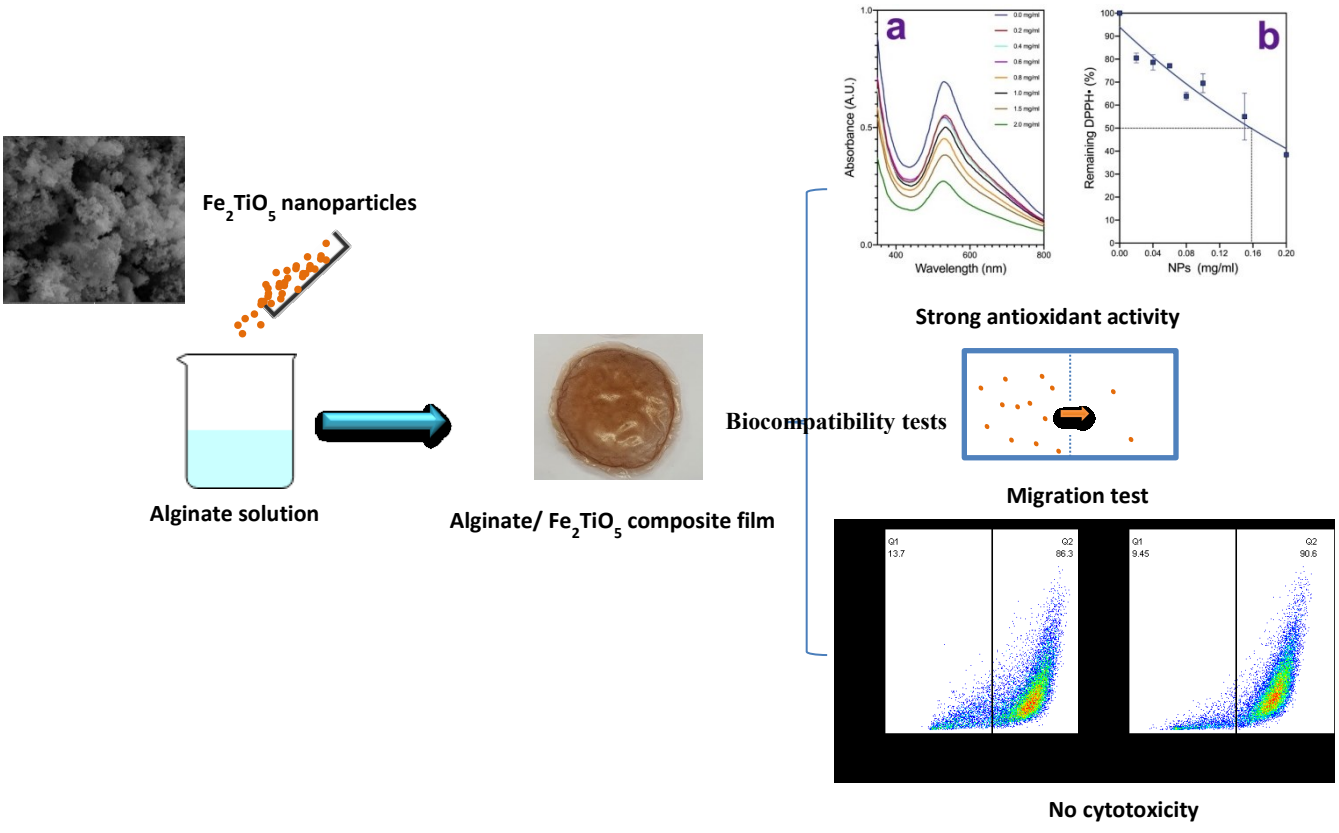

Abstract

An emerging technology of active packaging enables prolongation of food shelf life by limiting the oxygen transfer and the reactivity of free radicals, which both destruct food freshness. In this work, Fe_2TiO_5 nanoparticles were synthesized using a modified sol-gel method and evaluated as an enforcement of alginate food packaging film. Pure phase Fe_2TiO_5 nanoparticles had an average particle size of 44 nm and rhombohedral morphology. Fe_2TiO_5 nanoparticles induce no cell damage of human Caco-2 epithelial cells and show no inhibitory effect towards growth of a panel of bacterial strains, suggesting good biocompatibility. Films obtained by incorporation of Fe_2TiO_5 nanoparticles into alginate using the solvent casting method show no migration of iron or titanium ions from films to food simulants again suggesting their safety as a packaging material. Fe_2TiO_5 nanoparticles also showed strong antioxidant efficiency as determined using the $DPPH^{\cdot}$ assay, and confirmed further in a preservation test on fresh fruit.

Keywords: Fe_2TiO_5 nanoparticles; alginate film; composite film; antioxidant active; biocompatibility.

1. Introduction

Metal oxide nanoparticles (NPs), with a diameter ranging from 1-100 nm, have gained a lot of attention in the last decade in various fields ranging from catalysis, photocatalysis, sensors, biomedical applications and agri-food industry (Kannan et al. 2020; Nikolic et al. 2021). NPs used as food additives and food-contact materials have potential to improve quality and extend food shelf-live but need to be safe, cost-effective and eco-friendly. Potential risks of nanoparticles have aroused serious concerns of the public and in academia and have emphasized the need for engineering biocompatible inorganic nanomaterials.

Plastics are still widely used in food packaging due to their cheapness and longer durability. However, plastics cannot be recycled and cause an environmental crisis in the whole world (Ncube et al. 2020). Active packaging based on biocompatible polymers and metal oxide

NPs is under development in order to replace petroleum-based plastics and reduce the usage of preservatives (Peighambardoust et al. 2019; Priyadarshi and Rhim 2020). Alginate, as an alternative to plastics for food packaging, is a biocompatible, non-toxic, and an inexpensive biodegradable water-soluble polysaccharide, composed of mannuronic and glucuronic acid molecules bound by 1–4 glycosidic bonds. It can react with di- and trivalent cations forming crosslinks and becoming water-resistant which is of great importance for food packaging (Külcü 2020; Omerović et al. 2021). In addition, alginate exhibits low permeability to oxygen and vapours, flexibility, and good tensile strength (Jost et al. 2014). Metal oxide nanoparticles incorporated into alginate reinforced alginate packaging film through providing a strong antimicrobial activity, UV barrier, ethylene scavenging and smart sensing capacity (Nikolic et al. 2021). For instance, hydrothermally prepared Au-TiO_2 nanocomposites were dispersed into alginate solution and showed improved water resistance and antibacterial activity (Tang et al. 2018). Halloysite functionalized with ZnO nanoparticles have been incorporated into alginate films and showed a significant increase in the mechanical, water vapor barrier and UV light barrier properties (Shankar et al. 2018). Recent investigations have also included application of a $NiMn_2O_4$/alginate nano-biocomposite in temperature sensing (Dojcinovic et al. 2021), or Zn-MgO NPs/alginate in extending shelf life of smoked salmon (Vizzini et al. 2020). Even though the properties of metal oxide NPs are useful for food packaging, there is still a lack of using these nanomaterials regarding their changed physical and chemical properties compared with bulk materials, giving them the potential for causing a health risk to humans (Heo et al. 2020). Since May 2021, one of the most used metal oxide NPs in the food industry, TiO_2, has been banned from all food products in the Europe under the recommendation of the European Food Safety Authority (EFSA). Since June 2021, TiO_2 is no more considered as safe for use in animal

feed. On September 28, 2021 the Section: Novel Food and Toxicological Safety of the Food Chain of the Standing Committee on Plants, Animals, Food and Feed of the European Commission conducted an exchange of views and possible opinions on the timeline of the planned ban of TiO_2 food additive (E171). Pure TiO_2 NPs were shown to accumulate in the body after ingestion and to be potentially genotoxic (Luo et al. 2020). There is a need to replace TiO_2 by safer material for food industry applications.

Mixed metal oxide NPs, providing synergic physicochemical properties of their components and decreased toxicity are under intensive investigation for biological applications (Nikolic et al. 2021; Stankic et al. 2016). In the present work, we for the first time evaluate possible applications of Fe_2TiO_5 as a biocompatible food packaging material for alginate reinforcement. Fe_2TiO_5 (known as iron titanate or pseudobrookite) is a mixed metal oxide and chemically stable crystal (Vasiljevic et al. 2020a). It naturally occurs in titanium-rich volcanic rocks, and could be a good replacement for TiO_2. Fe_2TiO_5 has been identified as an intermediate between Fe_2O_3 and TiO_2 as it inherits a similar electronic and atomic structure to TiO_2 whilst its energy band gap is similar to Fe_2O_3 (2.2 eV). Recent research has focused on applying Fe_2TiO_5 as a promising photocatalyst material in natural sunlight for removal of pollutants, such as organic dyes (Vasiljevic et al. 2020a), photoanode for photoelectrochemical water splitting (Lee et al. 2020) or in gas sensing (Nikolic et al. 2018) but has not been evaluated in biological and agri-food applications. In view of promising photocatalytic properties of Fe_2TiO_5 and proven radical scavenging activity of TiO_2 (Ajmal et al. 2019) and Fe_2O_3 (Dowlath et al. 2021) we anticipate strong radical scavenging activity of Fe_2TiO_5. Through the combination of one highly reactive metal ion – Ti^{2+} and one highly biocompatible metal ion – Fe^{3+} (Stankic et al. 2016) in a

mixed metal oxide – Fe_2TiO_5 we hope for a cell friendly material, which is the first demand for future biodegradable active materials.

We assessed the biocompatibility of Fe_2TiO_5 using a human colorectal immortalized Caco-2 cell line and a model microbiome bacterium *Escherichia coli* as well as on a panel of environmental and pathogenic bacteria. In addition, to evaluate Fe_2TiO_5 as a food-contact material, we investigated the migration from Fe_2TiO_5/alginate nanocomposites into food simulants and its antioxidant activity. A preservation study conducted on fresh whole and cut strawberries in open atmosphere was performed to further assess the antioxidant activity of Fe_2TiO_5/alginate nanocomposite films. This study may contribute to development of novel cell friendly bimetallic oxide NPs that could replace TiO_2 NPs in active food packaging.

2. Materials and methods

2.1. Materials, reagents and solutions

Iron(III) nonahydrate ($Fe(NO_3)_3 \cdot 9\ H_2O$, ACS reagent, purity ≥98%), titanium isopropoxide ($Ti(OCH)(CH_3)_2$, purity 98%), oxalic acid (Puriss, purity ≥99%), citric acid monohydrate (ACS reagent, purity ≥99%), all from Sigma Aldrich (Darmstadt, Germany) were used for synthesis of the iron titanate (Fe_2TiO_5) nanoparticles. Alginic acid sodium salt (Sodium alginate) (Alfa Aesar, Thermo Fischer Scientific, Haverhill, Massachusetts, USA), calcium chloride (Lach-ner Chemicals, Neratovice, Czech Republic), glycerol (Galafarm, Belgrade, Serbia) and deionized water (Sigma Aldrich, Darmstadt, Germany) were used for alginate film preparation. Ethanol (Prolabo, Fontenay-sous-bois, France) and acetic acid (Prolabo, Fontenay-sous-bois, France) were used to prepared food simulants. 2,2 Diphenyl-1-picrylhydrazyl ($DPPH^{\cdot}$) (Sigma Aldrich, Saint Quentin Fallavier, France) and methanol (Prolabo, Fontenay-

sous-bois, France) were used in antioxidant tests. ZnO NPs of 50 nm average diameter (Sigma Aldrich, Saint Quentin Fallavier, France) were used in control toxicity tests.

2.2. Synthesis and characterisation of Fe_2TiO_5 nanoparticles

Iron titanate nanoparticle synthesis was conducted following a modified sol-gel method (Vasiljevic et al. 2020a). Iron(III) nonahydrate, titanium isopropoxide, oxalic acid (chelating agent) and citric acid (surfactant) were mixed on a magnetic mixer maintaining the temperature between 80-90 ^{o}C until a gel was formed. The formed gel was heated to 300 ^{o}C until a powder formed, and then calcined in a chamber furnace at 750 ^{o}C for 3 h. Structural characteristics of the obtained powder were investigated by measuring X-ray diffraction (range 2θ = 10-90^{o}, step 0.05s, acquisition rate 1^{o}/min, Rigaku Ultima IV diffractometer, Tokyo, Japan) and FT-IR spectrum (range 400-4000 cm^{-1}, FT-IR Nicolet 6700 ATR device, Waltham, MA, USA). The optical band gap was determined by measuring and analysing UV-Vis diffuse reflectance spectrum (Shimadzu UV-2600 with an ISR2600 Plus integrating sphere attachment, Kyoto, Japan). The powder morphology was investigated by Field emission electron microscopy - FESEM (TESCAN MIRA3 XM, Brno, Czech Republic) and transmission electron microscopy - TEM (JEM-2100 200 kV, JEOL Ltd. Tokyo, Japan). The specific surface area and pore structure were determined from measured N_2 adsorption-desorption isotherms (Micromeritics ASAP 2020, Norcross, GA, USA). Prior to measurement, the powder sample was degassed at 150 ^{o}C for 10 hours under reduced pressure.

2.3. Synthesis of alginate - Fe_2TiO_5 films

Alginate film was prepared using the previously described method (Vizzini et al. 2020). Briefly, 1.167 g of sodium alginate was mixed with 50 mL of deionized water for 6 h, then 1.5

mL of calcium chloride aqueous solution (5% w/v) and 1.5 mL of glycerol (100%) were added and the mixture was mixed for another 10 minutes. The formed solution was poured into a Petri dish and evenly spread in order to obtain alginate film. Alginate/NPs packaging films were obtained using the solvent casting method. For this, 55 mg of Fe_2TiO_5 nanoparticles (NPs) were added to the solution prepared in the same way and poured into a Petri dish to obtain alginate - Fe_2TiO_5 films. Both plates were incubated at 50 ^{o}C for 12 h. The film was wetted with a solution of 5% calcium chloride for 10 minutes, washed and dried and sterilized before utilization. A scheme of the film preparation is shown in Fig. S1. The film structure was observed by FT-IR spectroscopy in the range 4000-400 cm^{-1}, resolution 4 cm^{-1} (Perkin Elmer Spectrum Two, Waltham, MA, USA).

2.4. Bacterial strains

The bacterial strains used in this study are listed in Table S1. Strains were grown in brain-heart-infusion (BHI) medium, Becton Dickinson (DB, Le Pont de Claix, France), with shaking at 37 °C or on BHI agar at 37 °C. As described previously, the revitalization procedure of all cultures stored at −80 °C was conducted at 37 °C overnight in BHI broth, with the exception of *Campylobacter jejuni* (Zanet et al. 2019). *C. jejuni* was firstly incubated in a Columbia blood agar base (Thermo Fisher Scientific Inc., Illkirch, France) supplemented with 5% v/v of sheep defibrinated blood (Thermo Ficher Scientific Inc.) for 48 h under microaerophilic condition. Pure colonies of *C. jejuni* were then isolated on BHI agar medium and cultivated under microaerophilic condition as explained previously (Vizzini et al. 2021).

2.5. Antibacterial activity

Antibacterial activity of Fe_2TiO_5 NPs was tested by the standard disk diffusion method and through following the kinetics of bacterial growth (Auger et al. 2018; Vasiljevic et al. 2020b). The overnight-grown bacterial suspensions were standardized using the McFarland standard, and then spread onto the sterilized BHI agar dish. Whatman® filter paper circular disks of 5 mm diameter were placed on bacterial seeded plates and soaked with 15 µL of Fe_2TiO_5 NPs at different final concentrations (0.5, 1 and 5 mg/mL). Plates were incubated at 37 °C for 10–20 h, and the diameters of the inhibition zones were measured with a transparent ruler (Auger et al. 2018).

The antibacterial kinetics of Fe_2TiO_5 NPs (0.1, 1, and 2 mg/mL) against *Bacillus subtilis*, *Escherichia coli, Bacillus cytotoxicus* and *Salmonella enteritidis* were investigated using a diluted bacterial culture in fresh BHI medium to initial optical density at 600 nm (OD_{600}) of 0.1. Suspensions (200 µL each) were placed in 96 microplate wells and incubated at 37 °C. Bacterial growth was measured by following the OD_{600} overnight at 37 °C using the Infinite 200 PRO microplate reader (TECAN, Salzburg, Austria) as explained previously (Vasiljevic et al. 2020b). The absorbance of blanks containing the equivalent concentration of nanoparticles in BHI medium incubated under the same conditions was used to subtract the background absorption. A negative control was prepared replacing NPs with water. All data presented are the averages of at least triplicate measurements.

2.6. Ion migration

Ion migration was tested in two food simulant solutions (3% v/v acetic acid – HAc and 95% v/v ethanol - EtOH) that simulated acidic and fatty foods according to the European regulation (EU 10/2011), by placing 0.01 g film pieces into a container with 40 ml of the

solution. The samples were kept in the dark at 20 ^{o}C for 1, 3, 5, 7 and 10 days after which the pieces of film were removed from the solution, as described previously (Nikolic et al. 2021).

An inductively coupled plasma optical emission spectrometer (ICP-OES, Perkin Elmer Avio 2000, Waltham, MA, USA) was used to determine the concentrations of metal ion release from particle suspensions. Particle (film) suspensions for analysis were prepared in the following way: the solution was mixed with concentrated nitric acid, heated up in a water bath at 80-90 ºC, another 4 ml hydrogen peroxide was slowly added when the solution evaporated to 10 ml, and then evaporated until dry. Distilled water was slowly added until 40 ml with an additional 0.8 ml nitric acid to obtain a solution suitable for measurement. A calibration solution with distilled water was prepared in the same way. The prepared solutions were analysed for metal ion release by selecting the 238.204 line for Fe and the 334.940 line for Ti measurement. Concentrations of both cations were determined by the calibration curve method. The certified TraceCert 92091 Sigma-Aldrich multi-element standard was used for preparing the calibration curve.

2.7. *Antioxidant activity*

The antioxidant effect of the Fe_2TiO_5 NPs was evaluated through the DPPH$^{\cdot}$ colorimetric assay. DPPH$^{\cdot}$, a stable organic radical, dissolved in methanol shows an absorption peak at 517 nm, whose intensity decreases in the presence of a scavenger agent (Vasiljevic et al. 2020b). The minimum concentration of Fe_2TiO_5 NPs that inhibits 50% DPPH$^{\cdot}$ (EC_{50} value) was obtained by admixing particles in serial dilutions (0.2, 0.4, 0.6, 0.8, 1.0, 1.5 and 2 mg/ml) to 0.2 mM DPPH$^{\cdot}$ solution. The value of EC_{50} was expressed as molar ratio of NPs to DPPH$^{\cdot}$ radical. Antioxidant reducing power (ARP) which corresponds to number of moles of DPPH$^{\cdot}$ radical required to reduce 1 mol of NPs has been calculated as $1/EC_{50}$. The negative control was a solution of 0.2 mM DPPH$^{\cdot}$ where NPs were replaced with water. The mixtures were vortexed and left to stand

for 30 min in the dark before absorbance measuring against the blank using a UV-Vis spectrophotometer Biochrom Libra S22 (Serlabo Technologies, France). The radical scavenging activity (or antioxidant activity), expressed in % of $DPPH^{\cdot}$ inhibition, was calculated according to the following equation:

$$\text{Inhibition of } DPPH^{\cdot} (\%) = [(A_{blanc}(t)-A_{sample}(t)) / A_{blanc}(t)] \times 100, \quad (1)$$

where $A_{blanc}(t)$ represents the absorbance of $DPPH^{\cdot}$ solution without the addition of NPs at time t, and $A_{sample}(t)$ is the absorbance of $DPPH^{\cdot}$ solution containing NPs, at the same time. Kinetics test were carried out in triplicate.

2.8. Human cell line and flow cytometry measurements.

Caco-2 intestinal cells (ATCC HTB-37) were grown following ATCC recommendations at 37 °C in a humidified 10 % CO_2 atmosphere. To test cytotoxicity of Fe_2TiO_5 NPs, Caco-2 cells at 80% confluency were washed with Dulbecco's Modified Eagle Medium (DMEM) and incubated with the complete culture media containing NPs at 0.2, 0.5, 1 and 2 mg/mL for 24 h. Cell damage was quantified by acridine orange staining followed by flow cytometry analysis (LSRII LSR Fortessa X-20 (BD)) with the 488-nm laser line and the FITC (530/30) channel, as described previously (Vidic et al. 2014; Vidic et al. 2016). Briefly, cells were collected, washed in PBS and re-suspended in DMEM containing 0.1 µg/mL acridine orange dye. After incubated, stained cells were collected, washed and fixed with 3.5% paraformaldehyde in PBS for 30 min. The fixed cells were collected and re-suspended in PBS for analysis. Data were analyzed by using FlowJo Software (BD Biosciences).

2.9 Preservation study on fresh fruit

We purchased fresh strawberries from the local market to perform a preservation study of the Fe_2TiO_5/alginate composite film. The strawberries were placed on pieces of film, or strawberries were cut in half and covered by pieces of pure alginate or Fe_2TiO_5/alginate composite film. The study was conducted in open atmosphere at room temperature of around 20 °C and relative humidity of around 35%. Photographs were taken with high-resolution cameras for three consecutive days to register evidence of visible deterioration and microbial/fungal infection and growth.

3. Results and discussion

3.1. Structure, morphology textural and optical characteristics of Fe_2TiO_5 NPs

Structural parameters were determined by Rietveld refinement of the measured XRD patterns of the synthesized Fe_2TiO_5 powder with the GSAS II software package. The *Cmcm* space group was assumed and we used, as starting values in the refinement, the parameters determined for iron titanate synthesized with CTAB as the surfactant (Vasiljevic et al. 2020a). Phase pure Fe_2TiO_5 was obtained, with all diffraction peaks indexed to the orthorhombic phase of Fe_2TiO_5, space group *Cmcm*, as shown in Fig. 1. The determined lattice parameters were a = 3.73040(29), b = 9.7880(13) and c = 9.9633(11), while other unit cell parameters and atomic positions are given in Table S2. The crystallite size was determined using the Sherrer equation as 38 nm. In this case also, 72% iron ions showed a preference for 4c sites, with 64% occupying 8f sites similar to Fe_2TiO_5 synthesized using CTAB as the surfactant (Vasiljevic et al. 2020a), but lower than 75% noted by (Rodriguez et al, 2019), or 80% determined for Fe_2TiO_5 nanofibers obtained by electrospinning (Vasiljević et al. 2021).

FESEM and TEM images (Fig. 1b, c and d) showed that the Fe_2TiO_5 NPs were agglomerates or “clustered nanoparticles” formed of smaller particles with a rhombic shape. This

morphology can be due to coalescence of small particles into agglomerates (Nikolic et al. 2018; Vasiljevic et al. 2020a). The average particle size was estimated as 44 nm. This is slightly lower than 49.7 nm determined for Fe_2TiO_5 obtained using the sol-gel method (Vasiljevic et al. 2020a), or 80-140 nm for Fe_2TiO_5 obtained using solid state synthesis of starting nanosized oxide powders (Nikolic et al. 2018) and much lower than 0.8 μm for Fe_2TiO_5 obtained by solid state synthesis using starting microsized oxide powders (Rodrigues et al. 2019). Analysis of periodic lattice fringes in the high-resolution TEM (HRTEM) image (Fig. 1e) was performed using a fast Fourier transform (FFT). The lattice spacing of 0.49 nm was determined that corresponds to the (020) plane of an orthorhombic *Cmcm* structure and is in accordance with the parameters determined by the Rietveld refinement of the measured XRD pattern. This confirmed formation of phase pure uniform Fe_2TiO_5 nanoparticles.

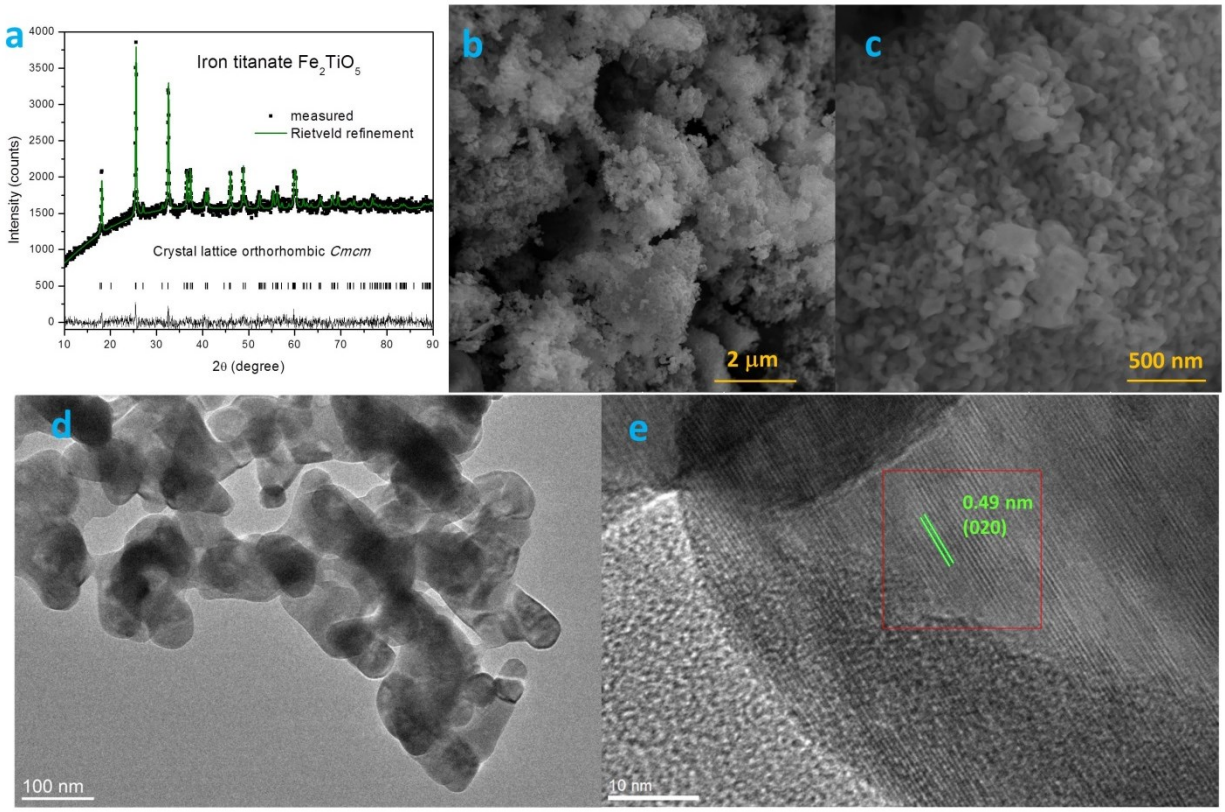

Fig. 1 Fe_2TiO_5 powder: a – X-ray diffraction pattern and Rietveld refinement, b, c – FESEM, d – TEM and e – HRTEM images

The textural properties (specific surface area and porosity) of the synthesized nanoparticles were determined by measuring nitrogen adsorption-desorption isotherms at 77 K. The measured N_2 adsorption/desorption curves (Fig. 2a) can be considered a type V isotherm, according to the IUPAC nomenclature (Thommes et al. 2015) that is characteristic for mesoporous materials. The specific surface area of Fe_2TiO_5 NPs was calculated by the Brunauer-Emmett-Teller (BET) method from the linear part of the N_2 absorption isotherm. A moderate value of 12.8 m^2/g was determined, slightly higher than when cetrimonium bromide (CTAB) was used as the surfactant (Vasiljevic et al. 2020a). The total pore volume at $p/p_0 = 0.998$ was 0.076 cm^3/g, originating mostly from mesopores with a volume of 0.074 cm^3/g calculated by the BET method from the desorption branch of the isotherm. The pore size distribution analysis showed that pore diameters ranged between 5 and 70 nm (Fig. 2a – inset), with a mean pore diameter (D_{mean}) of 25 nm and D_{max} of 22.9 nm, representing the diameter of pores occupying the maximal volume. In porous materials, interaction with atoms, ions and molecules is not only on the surface, but throughout the bulk of the material. Accordingly, TiO_2 with uniform mesoporous channels in the synthesized nanoparticles was shown to have increased number of highly accessible active sites, and enhanced efficiency (Li et al. 2014). Iron titanate synthesized here by the modified sol-gel method has a mesoporous pore structure with pores ranging from 5 to 70 nm and a moderate specific surface area.

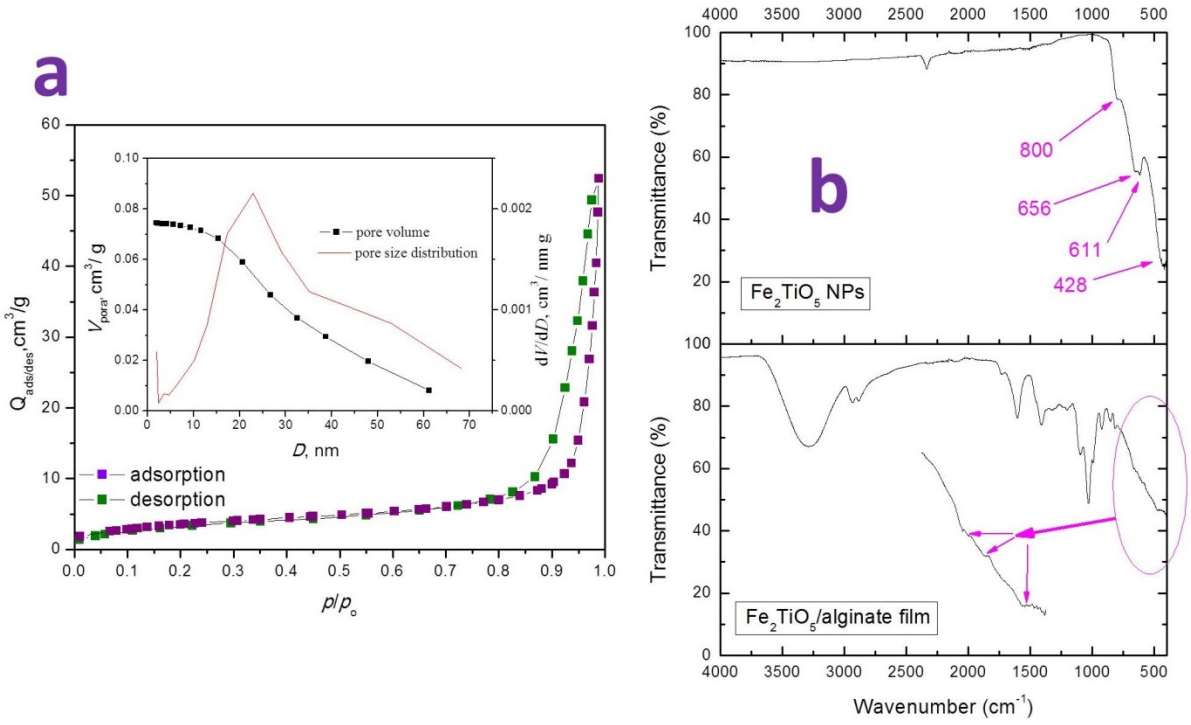

Fig. 2 Nitrogen adsorption-desorption isotherm and BET pore size distribution curves for Fe_2TiO_5NPs (a); FT-IR spectra (b) of Fe_2TiO_5 NPs (up) and Fe_2TiO_5-alginate film (down)

The absorbance spectrum was calculated from the measured diffraction reflection spectrum of Fe_2TiO_5 nanoparticles using the Kubelka-Munk approximation, given as an inset in Fig. S2. It shows that Fe_2TiO_5 NPs express strong visible light absorption capability. The direct optical band gap of Fe_2TiO_5 was estimated from the Tauc plot as 2.23 eV (Fig. S2) and is in accordance with previously obtained values for Fe_2TiO_5 NPs (Vasiljevic et al. 2020a).

3.2. FT-IR spectra of Fe_2TiO_5/alginate film

Measured FT-IR spectra of Fe_2TiO_5 NPs and the prepared Fe_2TiO_5/alginate film are shown in Fig. 2b. Only bands originating from vibrations of Fe^{3+}-O^{2-} and Ti^{4+}-O^{2-} groups belonging to Fe_2TiO_5 NPs can be noted in the NP spectrum at approximately 800, 656, 611 and 428 cm^{-1} (Salarizadeh et al. 2016; Vasiljevic et al. 2020a). Small bands in this region (400-800 cm^{-1}) remain (as marked in Fig. 2b, down) in the measured spectrum of the Fe_2TiO_5 alginate

film, confirming the presence of NPs in the film. Bands in the higher wavenumber region originate from sodium alginate film (Dojcinovic et al. 2021). Bands in the region 800-100 cm^{-1} can be attributed to mannuronic acid residues, C1-H mannuronic acid deformation and CO stretching of uronic acids. The prominent band at ~ 1032 is due to C-O stretching vibrations. COO^- symmetric and asymmetric stretching vibrations are noted at ~1400 and 1600 cm^{-1} originating from metal-carboxylate interactions, while the bands at ~2910 can be assigned to the CH anomer. The prominent O-H stretching band is noted at ~3292 cm^{-1} (Dojcinovic et al. 2021). The formation of such stretching bonds will have a significant effect on the physical and mechanical properties of packaging film. As shown in Fig. S1, the prepared Fe_2TiO_5/alginate film has a brown/reddish colour that is relatively uniform showing a relatively homogenous distribution of Fe_2TiO_5 nanoparticles in the alginate film.

3.3. ICP-OES measurement of ion release from Fe_2TiO_5/alginate films

Migration or release of ions from metal or metal oxide nanoparticles from packaging films into the packaged food product is one of the parameters that may determinate the film biocompatibility (Perera et al. 2021). The ions release depends on a variety of factors that include nanoparticle (size, solubility, diffusivity within the polymer), composition and packaging characteristics (polymer structure, viscosity), environmental conditions (temperature or mechanical stress), and food conditions including its pH value and hydrophobicity. Ion release is usually determined in food simulants (Nikolic et al. 2021; Perera et al. 2021). In this work, we evaluated Ti and Fe ion release from Fe_2TiO_5/alginate films into 3% (w/v) aqueous acetic acid and 95% (v/v) aqueous ethanol, at 20 °C for 10 days, sampling at day 1, 3, 5, 7 and 10. ICP-OES measurements performed on the prepared solutions showed that there was no Ti or Fe ion release into the food simulants, as all values determined were below the detection limit of the instrument

(in the range 0.001-0.032 mg/L). This is in accordance with previous analysis of Ti migration from other polymer matrixes such as chitosan (Enescu et al. 2020), or PET (Chen et al. 2019). In a recent review (Garcia et al. 2018) concluded that available research on nanoparticle migration, including Ti suggests that nanoparticles incorporated into polymers have a tendency to agglomerate and thus remain relatively firmly embedded in the polymer matrix.

3.4. Antioxidant effect

Incorporation of antioxidants in food packaging is a way to prevent spoilage of oxidation-sensitive food products. Antioxidant activity of Fe_2TiO_5 NPs was evaluated by the $DPPH^{\cdot}$ free radical assay. This assay is based on $DPPH^{\cdot}$ reduction to $DPPH_2$ by accepting a hydrogen atom from the antioxidant molecule, which changes the solution purple colour to yellow with concomitant decrease in absorbance at 517 nm. The observed $DPPH^{\cdot}$ radical scavenging activity of Fe_2TiO_5 NPs was dose dependent (Fig. 3a). Fig 3b displays the corresponding kinetics of antioxidant activity of NPs (as calculated from equation (1)), with the concentration EC_{50} of 0.16 mg/mL required to decrease the initial $DPPH^{\cdot}$ concentration by 50% (0.66 μM, molecular weight of Fe_2TiO_5 is 239.46 g/mol). The calculated $ARP_{\mu M}$ was 1.5. Such strong scavenging activity of Fe_2TiO_5 NPs is similar to those previously reported for TiO_2 NPs (0.1 mg/mL) of similar sizes (Ajmal et al. 2019). Interestingly, the hydrogen ions availability is probably high in aqueous solutions of two nanoparticles since we found that pH of 1 mg/mL Fe_2TiO_5 NPs and 1 mg/mL TiO_2 was 2, and 4.5, respectively. Hematite (α-Fe_2O_3) has also previously shown free radical scavenging activity (EC_{50} 0.18 mg/mL) that has been attributed to electron transfer towards the free radical located at the nitrogen atom in DPPH (Bhattacharya et al. 2014; Dowlath et al. 2021). Thus, iron titanate (Fe_2TiO_5) that combines characteristics of both TiO_2 and Fe_2O_3 NPs

shows strong antioxidant activity that was not controlled by metal ions release rate, but by the surface reactivity of NPs.

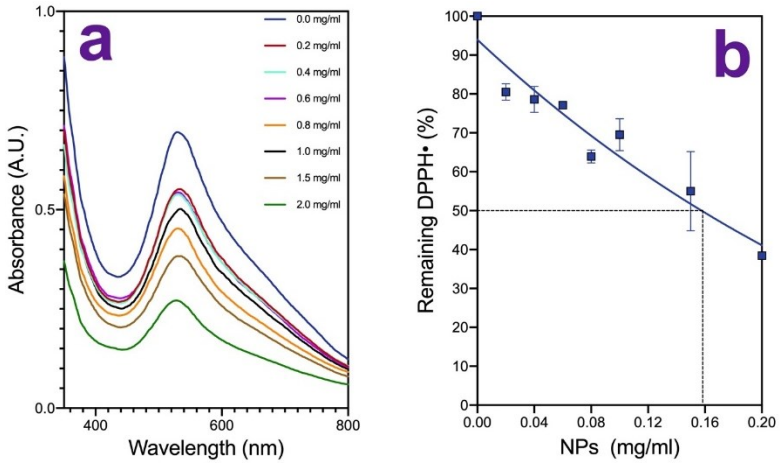

Fig. 3. DPPH˙ assay showing antioxidant activity of Fe_2TiO_5 NPs with EC_{50} 0.16 mg/mL (a) adsorption curves obtained with increasing concentrations of NPs. (b) EC_{50} plot.

3.5. Biocompatibility of Fe_2TiO_5 NPs

In order to test the biocompatibility of Fe_2TiO_5 NPs, the human epithelial Caco-2 cells were incubated with different concentrations of the NPs (0.2 mg/ml - 2 mg/ml), stained with acridine orange and analysed by flow cytometry. Acridine orange fluorescence dye easily traverses the cell membrane and accumulates in lysosomes of live cells. During necrosis, when structural integrity of cell membranes is lost, lysosomes are ruptured and red fluorescence of acridine orange decreases. No significant decrease in acridine orange staining was observed in cells incubated with NPs compared to the control cells incubated with PBS (Fig. 4). This strongly suggests that Fe_2TiO_5 caused no cell damage. For comparison, 0.5 mg/ml ZnO NPs decreased fluorescent staining indicating that cells were necrotic. These findings suggest the biocompatibility of Fe_2TiO_5 NPs at concentrations $\leq$ 2 mg/mL.

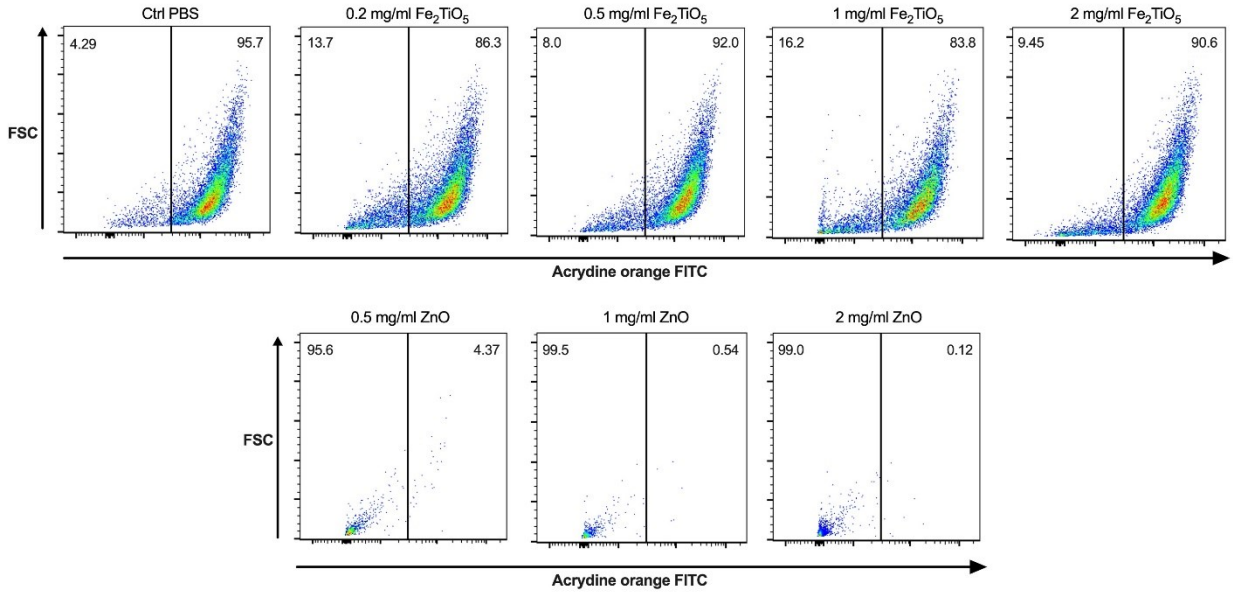

Fig. 4. Acridine orange staining and flow cytometry representative plots (n = 3) of control Caco-2 cells and Caco-2 cells incubated with different concentrations of Fe_2TiO_5 NPs and ZnO NPs for 24 h. For all plots, numbers indicate percentage of cells in relevant gate.

Since cell membranes are negatively charged, cytotoxicity of metal oxides NPs is greatly influenced by their surface charges (Auger et al. 2019; Valgimigli et al. 2018). Positively charged NPs are usually more toxic to plasma membrane than negatively surface charged NPs (Auger et al. 2019; Fröhlich 2012). The zeta potential value of Fe_2TiO_5 NPs in deionized water was determined in our previous work showing a negative value (−21.6 ± 6.8) mV (Vasiljevic et al. 2020a). In contrast with Fe_2TiO_5 NPs analyzed in this work, and Fe oxide NPs, such as α-Fe_2O_3 and Fe_3O_4 NPs (Stankic et al. 2016; Vihodceva et al. 2021), pure TiO_2 NPs were shown to exhibit cytotoxicity, induce DNA damages and modify ATP-binding cassette (ABC) family xenobiotic efflux pumps in human Caco2 cells (Dorier et al. 2019; Gerloff et al. 2012). The toxic effect was highly dependent on the TiO_2 particles' size, morphology, crystal structure and amount of surface defects.

3.6. Antibacterial effect of Fe_2TiO_5 NPs

We next sought to evaluate for potential cytotoxicity of Fe_2TiO_5 NPs towards *E. coli,* as a model of microbiota and environmental Gram-negative bacteria and *B. subtilis,* as a model of environmental Gram-positive bacteria. Different concentrations of Fe_2TiO_5 were studied by measuring growth kinetics of two bacteria in the BHI medium using a plate reader (Fig. 5). UV irradiation was performed before incubation. No antibacterial effect was observed for NPs concentrations ≤ 2 mg/mL. In case of *B. subtilis* a decrease of absorbance was observed after 7 h of incubation even in the absence of NPs probably due to the lower availability of oxygen in microplates (semi-anaerobiosis condition). In contrast, *E. coli* is a facultative anaerobic bacterium, able to grow in both aerobic and anaerobic environments.

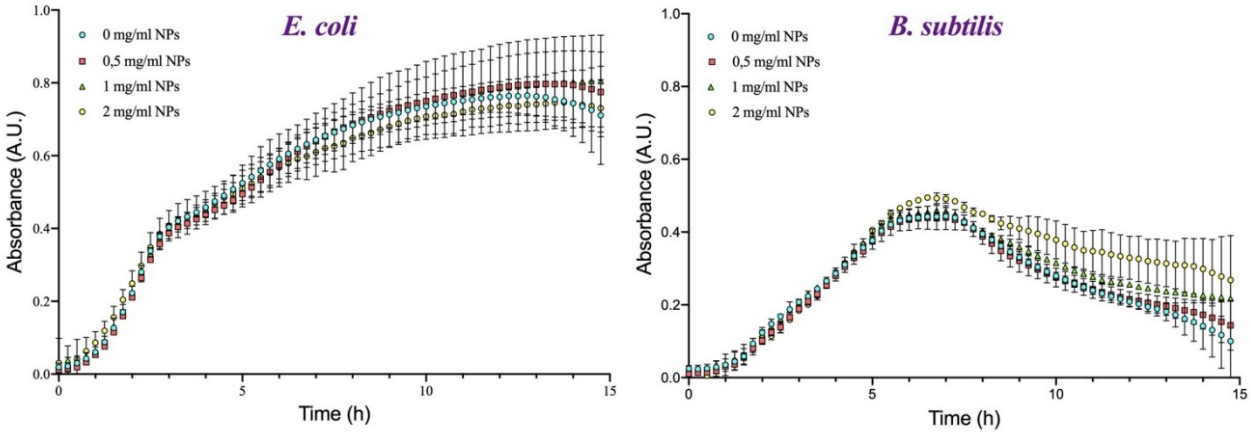

Fig. 5 Growth kinetics of *E. coli* and *B. subtilis* alone or in the presence of different concentrations of Fe_2TiO_5 nanoparticles in BHI.

To confirm that Fe_2TiO_5 NPs show no toxicity towards bacterial cells, a panel of strains, listed in Table S1, was tested by following growing kinetics in the presence of NPs (Fig. S3) and by the disk diffusion method. Both tests indicated no toxicity of negatively surface charged

Fe_2TiO_5 NPs for concentration ≤ 5 mg/mL, i.e., concentrations much superior of those providing a strong antioxidant efficiency.

Interestingly, TiO_2 NPs of different sizes, morphology or crystal structures have been reported to exhibit marked antibacterial activity allowing efficient eradication of various bacterial strains (Stankic et al. 2016). Antibacterial activity has been reported for other metal oxides, such as ZnO, MgO and is strongly influenced by their composition, size, shape and crystal structure (Nikolic et al. 2021). Compared to TiO_2, negatively charged hematite (α-Fe_2O_3) NPs did not exhibit antimicrobial activity against *E. coli* or *S. aureus* in deionized water up to concentrations of 1mg/ml, while some antibacterial activity was noted for positively charged hematite NPs against *E. coli*, but not *S. aureus* (Vihodceva et al. 2021). Fe_2TiO_5 NPs produced here, also negatively charged in water (Vasiljevic et al. 2020a), showed higher biocompatibility towards both bacterial and human cells tested.

3.7 Preservation of fruit

To verify the preservation effect of Fe_2TiO_5/alginate on a food sample sensitive to oxidation the preservation test was performed on cut and whole strawberries in open air conditions. Open air was used as it deteriorates fruit integrity (Vargas-Torrico et al. 2022). In the case of whole strawberries placed on pieces of alginate or Fe_2TiO_5/alginate composite film (Fig. 6A) there was no significant noticeable change on day 1, though on day 2 the ripening process started on all fruit samples, but most noticeably on the control sample (Fig. S4A). On day 3, visible deterioration was noticeable on the control sample, including evident textural damage, tissue degradation and visible growth of mould. The strawberry sample placed on alginate film also showed such damage, though tissue degradation was slightly less. The Fe_2TiO_5/alginate

composite film has acted as a barrier delaying the rotting process and reducing the tissue degradation rate.

Cut strawberry spoils fast in open air conditions, and deterioration started on day 1 on the control sample, with slight curling of the edges (Fig. 6B, Fig. S4B). The cut strawberry samples covered with alginate or Fe_2TiO_5/alginate composite film showed no visible deterioration on day 1. This was more noticeable on day 2 when the fruit tissue started to brown on the control sample. On day 3 there was visible deterioration and fungal growth noticeable on the cut strawberry control sample (Fig. 6B, Fig. S4B), while the alginate film provided some protection in that tissue degradation had started and edge discoloration and deterioration was more noticeable, but was less than in the control sample.

A	Control	Alginate film	Fe_2TiO_5/algin. film
Day 0			
Day 3		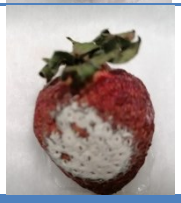	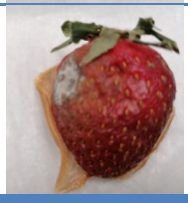
B	**Control**	**Alginate film**	**Fe_2TiO_5/algin. film**
Day 0			
Day 1			

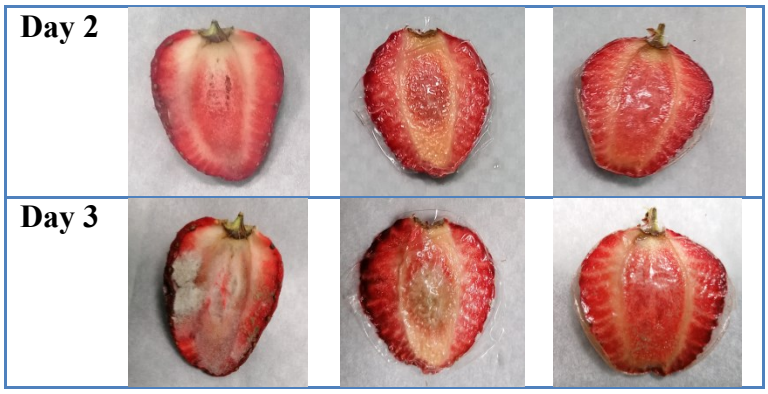

Fig. 6 Preservation study: (A) Conservation study of whole strawberries, (B) Conservation study of cut strawberries.

4. Conclusion

We produced active alginate composite films by incorporating Fe_2TiO_5 NPs via the solvent-casting method to develop active biocompatible films. As synthetized, pure phase Fe_2TiO_5 NPs were mesoporous with an average particle size of 44 nm. The strong radical scavenging activity of Fe_2TiO_5 NPs observed in the DPPH tests suggests that its utilization in food packaging may prevent spoilage of oxidation sensitive food products. The ICP-OES measurements indicated no metal ion migration from alginate/Fe_2TiO_5 NPs to food simulants, which suggests the biocompatibility of the film. Moreover, nanoparticles alone showed no cytotoxicity as no inhibition of bacterial growth not human Caco-2 cells damage was observed in the presence of Fe_2TiO_5 NPs up to 5 mg/mL. This work is the first step in the evaluation of Fe_2TiO_5 NPs as a food-contact material. The protective antioxidant activity of this packaging film in a real food system was tested and confirmed in a preservation study of fresh whole and cut strawberries. Finally, the mesoporous structure of Fe_2TiO_5 nanocrystals suggests that they can be used as carriers to integrate other active compounds in the film, such as antibacterial peptides or essential oils, and to provide packaging films with multiple activities for prolonged shelf-life of various foods.

Credit author statement

Francesco Rizzotto: Investigation and analysis of antioxidant, human cell line and antibacterial activity; Writing – original draft; Zorka Z. Vasiljevic: Synthesis and analysis of Fe_2TiO_5 nanoparticles and Fe_2TiO_5 embedded alginate films; Preservation test; UV/Vis measurement and analysis, Writing – original draft, Writing-review and editing, Visualization; Gordana Stanojevic, Ion migration measurement and analysis; Milena P. Dojcinovic, Investigation of Fe_2TiO_5 embedded alginate films, ion migration analysis; Writing-review and editing; Ivona Jankovic-Castvan, Nitrogen porosimetry measurement and analysis; Jelena D. Vujancevic, FESEM image measurement and analysis; Nenad B. Tadic, XRD measurement; G. O. Brankovic TEM measurement and analysis; Aurélie Magniez, flow cytometry measurements and analysis; Jasmina Vidic: Conceptualization, Supervision, Writing - Original draft, Writing-review and editing; Maria Vesna Nikolic: Conceptualization, Visualization, FT-IR measurements and analysis, Preservation test, Writing – Original draft, Writing-review and editing.

Declaration of competing interests

The authors declare that they have no known competing financial interests or personal relationships that could have appeared to influence the work reported in this paper.

Acknowledgements

The authors are grateful to Jugoslav Krstic (IHTM, Serbia) for valuable advice concerning ICP measurements, Goran Lakisic (INRAE, France) for valuable help with Caco2 cells. We are also grateful to Sandrine Auger (INRAE, France) for kindly gift of *B. cytotoxicus* and Florence Dubois-Brissonnet (AgroParisTech, France) for kindly gift of *Salmonella* strain. Z.Z.V., G.S., M.P.D., G.O.B. and M.V.N. are grateful for funding grant 451-03-9/2022-68/200053 and J.D.V. for the funding grant 451-03-9/2022-68/200175 from the Ministry for Education, Science and Technological Development of the Republic of Serbia. J.V. and F.R. acknowledge the European Union support through the Horizon 2020 research and innovation programme under the Marie Sklodowska-Curie grant agreement 872662 (IPANEMA). The TEM work was conducted in the Centre for Electron Microscopy and Microanalysis (CEMM) at the Jožef Štefan Institute, Ljubljana (Slovenia).

Appendix A: Supplementary data

References

Ajmal, N., Saraswat, K., Bakht, M.A., Riadi, Y., Ahsan, M.J., Noushad, M., 2019. Cost-effective and eco-friendly synthesis of titanium dioxide (TiO2) nanoparticles using fruit's peel agro-waste extracts: characterization, in vitro antibacterial, antioxidant activities. Green Chemistry Letters and Reviews 12(3), 244-254.

Auger, S., Henry, C., Péchaux, C., Lejal, N., Zanet, V., Nikolic, M.V., Manzano, M., Vidic, J., 2019. Exploring the impact of Mg-doped ZnO nanoparticles on a model soil microorganism Bacillus subtilis. Ecotoxicology and Environmental Safety 182, 109421.

Auger, S., Henry, C., Péchoux, C., Suman, S., Lejal, N., Bertho, N., Larcher, T., Stankic, S., Vidic, J., 2018. Exploring multiple effects of Zn 0.15 Mg 0.85 O nanoparticles on Bacillus subtilis and macrophages. Scientific reports 8(1), 1-14.

Bhattacharya, K., Gogoi, B., Buragohain, A., Deb, P., 2014. Fe2O3/C nanocomposites having distinctive antioxidant activity and hemolysis prevention efficiency. Materials Science and Engineering: C 42, 595-600.

Chen, J., Dong, X., Zhang, Q., Ding, S., 2019. Migration of titanium dioxide from PET/TiO2 composite film for polymer-laminated steel. Food Additives & Contaminants: Part A 36(3), 483-491.

Dojcinovic, M.P., Vasiljevic, Z.Z., Kovac, J., Tadic, N.B., Nikolic, M.V., 2021. Nickel Manganite-Sodium Alginate Nano-Biocomposite for Temperature Sensing. Chemosensors 9(9), 241.

Dorier, M., Béal, D., Tisseyre, C., Marie-Desvergne, C., Dubosson, M., Barreau, F., Houdeau, E., Herlin-Boime, N., Rabilloud, T., Carrière, M., 2019. The food additive E171 and titanium dioxide nanoparticles indirectly alter the homeostasis of human intestinal epithelial cells in vitro. Environmental Science: Nano 6(5), 1549-1561.

Dowlath, M.J.H., Musthafa, S.A., Khalith, S.M., Varjani, S., Karuppannan, S.K., Ramanujam, G.M., Arunachalam, A.M., Arunachalam, K.D., Chandrasekaran, M., Chang, S.W., 2021. Comparison of characteristics and biocompatibility of green synthesized iron oxide nanoparticles with chemical synthesized nanoparticles. Environmental Research 201, 111585.

Enescu, D., Dehelean, A., Goncalves, C., Cerqueira, M.A., Magdas, D.A., Fucinos, P., Pastrana, L.M., 2020. Evaluation of the specific migration according to EU standards of titanium from Chitosan/Metal complexes films containing TiO2 particles into different food simulants. A comparative study of the nano-sized vs micro-sized particles. Food Packaging and Shelf Life 26, 100579.

Fröhlich, E., 2012. The role of surface charge in cellular uptake and cytotoxicity of medical nanoparticles. International journal of nanomedicine 7, 5577.

Garcia, C.V., Shin, G.H., Kim, J.T., 2018. Metal oxide-based nanocomposites in food packaging: Applications, migration, and regulations. Trends in food science & technology 82, 21-31.

Gerloff, K., Fenoglio, I., Carella, E., Kolling, J., Albrecht, C., Boots, A.W., Förster, I., Schins, R.P., 2012. Distinctive toxicity of TiO2 rutile/anatase mixed phase nanoparticles on Caco-2 cells. Chemical research in toxicology 25(3), 646-655.

Heo, M.B., Kwak, M., An, K.S., Kim, H.J., Ryu, H.Y., Lee, S.M., Song, K.S., Kim, I.Y., Kwon, J.-H., Lee, T.G., 2020. Oral toxicity of titanium dioxide P25 at repeated dose 28-day and 90-day in rats. Particle and Fibre Toxicology 17(1), 1-22.

Jost, V., Kobsik, K., Schmid, M., Noller, K., 2014. Influence of plasticiser on the barrier, mechanical and grease resistance properties of alginate cast films. Carbohydrate polymers 110, 309-319.

Kannan, K., Radhika, D., Sadasivuni, K.K., Reddy, K.R., Raghu, A.V., 2020. Nanostructured metal oxides and its hybrids for photocatalytic and biomedical applications. Advances in Colloid and Interface Science 281, 102178.

Külcü, İ.D., 2020. A Constitutive model for alginate-based double network hydrogels cross-linked by mono-, di-, and trivalent cations. Gels 7(1), 3.

Lee, D., Baltazar, V.U., Smart, T.J., Ping, Y., Choi, K.-S., 2020. Electrochemical oxidation of metal–catechol complexes as a new synthesis route to the high-quality ternary photoelectrodes: A case study of fe2tio5 photoanodes. ACS Applied Materials & Interfaces 12(26), 29275-29284.

Li, W., Wu, Z., Wang, J., Elzatahry, A.A., Zhao, D., 2014. A perspective on mesoporous TiO2 materials. Chemistry of materials 26(1), 287-298.

Luo, Z., Li, Z., Xie, Z., Sokolova, I.M., Song, L., Peijnenburg, W.J., Hu, M., Wang, Y., 2020. Rethinking nano-TiO2 safety: overview of toxic effects in humans and aquatic animals. Small 16(36), 2002019.

Ncube, L.K., Ude, A.U., Ogunmuyiwa, E.N., Zulkifli, R., Beas, I.N., 2020. Environmental impact of food packaging materials: A review of contemporary development from conventional plastics to polylactic acid based materials. Materials 13(21), 4994.

Nikolic, M.V., Vasiljevic, Z.Z., Auger, S., Vidic, J., 2021. Metal oxide nanoparticles for safe active and intelligent food packaging. Trends in Food Science & Technology 116, 655-668.

Nikolic, M.V., Vasiljevic, Z.Z., Lukovic, M.D., Pavlovic, V.P., Vujancevic, J., Radovanovic, M., Krstic, J.B., Vlahovic, B., Pavlovic, V.B., 2018. Humidity sensing properties of nanocrystalline pseudobrookite (Fe2TiO5) based thick films. Sensors and Actuators B: Chemical 277, 654-664.

Omerović, N., Djisalov, M., Živojević, K., Mladenović, M., Vunduk, J., Milenković, I., Knežević, N.Ž., Gadjanski, I., Vidić, J., 2021. Antimicrobial nanoparticles and biodegradable polymer composites for active food packaging applications. Comprehensive Reviews in Food Science and Food Safety 20(3), 2428-2454.

Peighambardoust, S.J., Peighambardoust, S.H., Pournasir, N., Pakdel, P.M., 2019. Properties of active starch-based films incorporating a combination of Ag, ZnO and CuO nanoparticles for potential use in food packaging applications. Food Packaging and Shelf Life 22, 100420.

Perera, K.Y., Jaiswal, S., Jaiswal, A.K., 2021. A review on nanomaterials and nanohybrids based bio-nanocomposites for food packaging. Food Chemistry, 131912.

Priyadarshi, R., Rhim, J.-W., 2020. Chitosan-based biodegradable functional films for food packaging applications. Innovative Food Science & Emerging Technologies 62, 102346.

Rodrigues, J.E., Rosa, W.S., Ferrer, M.M., Cunha, T.R., Zapata, M.J.M., Sambrano, J.R., Martinez, J.L., Pizani, P.S., Alonso, J.A., Hernandes, A.C., 2019. Spin-phonon coupling in uniaxial anisotropic spin-glass based on Fe2TiO5 pseudobrookite. Journal of Alloys and Compounds 799, 563-572.

Salarizadeh, P., Javanbakht, M., Pourmahdian, S., Bagheri, A., Beydaghi, H., Enhessari, M., 2016. Surface modification of Fe2TiO5 nanoparticles by silane coupling agent: Synthesis and application in proton exchange composite membranes. Journal of colloid and interface science 472, 135-144.

Shankar, S., Kasapis, S., Rhim, J.-W., 2018. Alginate-based nanocomposite films reinforced with halloysite nanotubes functionalized by alkali treatment and zinc oxide nanoparticles. International journal of biological macromolecules 118, 1824-1832.

Stankic, S., Suman, S., Haque, F., Vidic, J., 2016. Pure and multi metal oxide nanoparticles: synthesis, antibacterial and cytotoxic properties. Journal of nanobiotechnology 14(1), 1-20.

Tang, S., Wang, Z., Li, P., Li, W., Li, C., Wang, Y., Chu, P.K., 2018. Degradable and photocatalytic antibacterial Au-TiO2/sodium alginate nanocomposite films for active food packaging. Nanomaterials 8(11), 930.

Valgimigli, L., Baschieri, A., Amorati, R., 2018. Antioxidant activity of nanomaterials. Journal of Materials Chemistry B 6(14), 2036-2051.

Vasiljevic, Z., Dojcinovic, M., Vujancevic, J., Jankovic-Castvan, I., Ognjanovic, M., Tadic, N., Stojadinovic, S., Brankovic, G., Nikolic, M., 2020a. Photocatalytic degradation of methylene blue under natural sunlight using iron titanate nanoparticles prepared by a modified sol–gel method. Royal Society open science 7(9), 200708.

Vasiljevic, Z.Z., Dojcinovic, M.P., Krstic, J.B., Ribic, V., Tadic, N.B., Ognjanovic, M., Auger, S., Vidic, J., Nikolic, M.V., 2020b. Synthesis and antibacterial activity of iron manganite (FeMnO 3) particles against the environmental bacterium Bacillus subtilis. RSC Advances 10(23), 13879-13888.

Vasiljević, Z.Ž., Dojčinović, M.P., Vujančević, J.D., Spreitzer, M., Kovač, J., Bartolić, D., Marković, S., Janković-Častvan, I., Tadić, N.B., Nikolić, M.V., 2021. Exploring the impact of calcination parameters on the crystal structure, morphology, and optical properties of electrospun Fe 2 TiO 5 nanofibers. RSC Advances 11(51), 32358-32368.

Vidic, J., Richard, C.-A., Péchoux, C., Da Costa, B., Bertho, N., Mazerat, S., Delmas, B., Chevalier, C., 2016. Amyloid assemblies of influenza A virus PB1-F2 protein damage membrane and induce cytotoxicity. Journal of Biological Chemistry 291(2), 739-751.

Vihodceva, S., Šutka, A., Sihtmäe, M., Rosenberg, M., Otsus, M., Kurvet, I., Kasemets, K., 2021. Antibacterial activity of positively and negatively charged hematite (α-Fe2O3) nanoparticles to Escherichia coli, Staphylococcus Aureus and Vibrio Fischeri. Nanomaterials, 2021 (11), 652. s Note: MDPI stays neutral with regard to jurisdictional claims in published ….

Vizzini, P., Beltrame, E., Zanet, V., Vidic, J., Manzano, M., 2020. Development and evaluation of qPCR detection method and Zn-MgO/alginate active packaging for controlling Listeria monocytogenes contamination in cold-smoked salmon. Foods 9(10), 1353.

Vizzini, P., Manzano, M., Farre, C., Meylheuc, T., Chaix, C., Ramarao, N., Vidic, J., 2021. Highly sensitive detection of Campylobacter spp. In chicken meat using a silica nanoparticle enhanced dot blot DNA biosensor. Biosensors and Bioelectronics 171, 112689.

Zanet, V., Vidic, J., Auger, S., Vizzini, P., Lippe, G., Iacumin, L., Comi, G., Manzano, M., 2019. Activity evaluation of pure and doped zinc oxide nanoparticles against bacterial pathogens and Saccharomyces cerevisiae. Journal of applied microbiology 127(5), 1391-1402.